Demonstration of Separation Control Using Dielectric Barrier Discharge Plasma Actuators

Lennart S. Hultgren and David E. Ashpis
NASA John H. Glenn Research Center, Cleveland, Ohio 44135

I. Introduction

THIS Note reports the results of an experimental study of active flow control of boundary-layer separation with a novel phased-array dielectric barrier discharge (DBD) plasma actuator. The flow of interest is flow over the suction surface of a low-pressure turbine (LPT) airfoil: specifically, the "Pak-B" airfoil that was the subject of many prior studies (e.g., [1]).

Typically, the LPT airfoil boundary layers are turbulent and fully attached at sea-level takeoff conditions; whereas at cruise conditions, a substantial fraction of the boundary layers may be transitional because the Reynolds number is low due to the lower density at altitude [2]. The strong adverse pressure gradients on the suction side of these airfoils can lead to boundary-layer separation. Large separation bubbles, particularly those that fail to reattach, cause a significant degradation of engine efficiency [2–4]. A component efficiency drop on the order of 2% may occur between takeoff and cruise conditions for large commercial transport engines and 7% for smaller engines at higher altitude; hence, there is a large benefit in mitigating the separation.

LPT flows are unique, being characterized by a low Reynolds number, high levels of freestream turbulence, and passing wakes. As studied in [5–7], there is an intricate interplay between separation and transition. Transition may begin before or after separation, depending on the pressure distribution, Reynolds number, and other flow conditions. If the transition occurs early in the boundary layer, then separation may be reduced or completely eliminated. Transition in the shear layer of a separation bubble can lead to rapid reattachment. This suggests using flow control mechanisms to trigger and enhance early transition, leading to separation delay or elimination.

A review of flow control in fluid mechanics was provided by Gad-el-Hak [8]. A recent comprehensive review by Tiainen et al. [9] was motivated by separation control in compressors. Overviews of separation control specific to the LPT were included by Volino [10] and Sondergaard [11]. The techniques included passive approaches [11–13] and active approaches employing steady and pulsed vortex-generating jets [10,11,14–20]. Passive devices optimized for separation control at low Reynolds numbers tended to increase losses at high Reynolds numbers [10]. Active devices had the attractive feature that they could be used only when needed and would not affect the flow when turned off.

Our focus is on active flow control employing dielectric barrier discharge (DBD) plasma actuators, which are now a well-known technology that was extensively studied in the recent 15–20 years and was well summarized in a series of review papers [21–28]. Initially, the actuators were named glow discharge actuators [29] but, later on, Enloe et al. [30] identified the underlying physical mechanisms as DBD. As time progressed, the term AC-DBD (for alternating current DBD) was coined for actuators operating typically in the 1–20 kHz range and provide a control mechanism by generating momentum with little heating, whereas the term NS-DBD (for nanosecond DBD) was used for actuators operating with repetitive short nanosecond-scale pulses that provide control via intense localized heating (but could also generate momentum) [31–33]. DBD actuators are purely electronic surface-mounted devices, and therefore have advantages over jet actuators.

The majority of studies on DBD flow control in the literature were focused on external flows, and only a relatively small number of experimental studies employing AC-DBD actuators targeted LPT separation. Several experiments were performed in single-passage facilities that simulated LPT airfoils. Boxx et al. [34] used a flat plate subject to an imposed pressure gradient. Burman et al. [35,36] used a single Pak-B passage with and without passing wakes. Matsunuma and Segawa [37] and Pescini et al. [38] used curved walls that produced representative LPT pressure distribution. Studies in linear cascade facilities were performed by List et al. [39] in a Langston airfoil cascade (not LPT), and Huang et al. [40,41] performed extensive studies in a Pak-B LPT airfoil cascade and compared them to vortex generators. Marks et al. [42] performed wind-tunnel tests on an Eppler 387 airfoil and compared three AC-DBD actuator topologies. Although it was a wing airfoil, it exhibited low-Reynolds-number separation at midchord, which was similar to the LPT.

In the work reported here, we use a unique phased-array plasma actuator for which the design follows the novel idea of Corke and Matlis [43]. It is an AC-DBD actuator, constructed of several pairs of individual electrodes, that generates travelling waves without the need to individually control each electrode pair. Travelling wave actuators were used in [44–46], and they involved powering and synchronizing several individual electrode pairs. In contrast, the present arrangement uses detuned signals applied to each electrode pair and naturally generates a travelling discharge wave with a beat frequency that is in the frequency range of Kelvin–Helmholtz instability waves in the shear layer of the separated region. Excitation of the instability waves results in the flow control mechanism that suppresses the separation. Corke and Matlis, in [43], fabricated a phased-array actuator and provided a proof of concept, and they demonstrated a cylindrical version of the actuator to control instability modes in a circular jet. Post [47] later showed that an asymmetric configuration improved on the symmetric configuration used in [43]. To our knowledge, this actuator type was not further used since then, and the work reported here is the first to employ the phased-array actuator for active flow control of a separated boundary layer [48].

II. Experimental Setup

The experiments were conducted in a low-speed recirculating wind tunnel. It was used in earlier studies [6,49]. A two-dimensional contoured surface on the upper wall induced the desired Pak-B suction surface pressure gradient on an acrylic flat plate mounted in the test section (Fig. 1). A streamwise section of length $L_s =$ 207.55 mm on the flat test surface simulated the airfoil suction

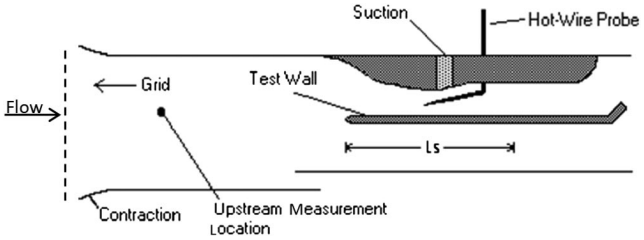

Fig. 1 Schematic of the test section; $L_s = 208$ mm.

surface, as in [6]. Turbulence grids established the turbulence intensity (TI) to about 0.2 and 2.5%, measured in the test section inlet and normalized with the exit velocity. The high-TI case represents a realistic value of TI in LPTs, which was reported to be as low as about 3% [50]. The experimental setup was described in detail in [51]; the following subsections provide a brief summary.

A. Actuator

A phased-plasma-array actuator, similar to [43] but with asymmetric and offset electrode pairs (Fig. 2), was surface flush mounted just upstream of the separation point. The actuator was fabricated using printed-circuit-board technology; five of its seven spanwise-oriented electrode pairs were used. The top electrodes were, in turn, fed a sequence of (positive) pulses with a repeat rate of $f_t = 4$ kHz. The common bottom electrodes were fed a pulse train of opposite polarity (negative) with a slightly different repeat rate f_b. The frequency difference (or detuning) of $\Delta f = f_t - f_b$ gave rise to the beat frequency of the DBD plasma. A negative Δf value indicated that the plasma formed sequentially and repeatedly in the downstream direction, and a positive value yielded propagation in the upstream direction. The voltage difference across an active electrode pair was 3.84 kV. Figure 3 shows a schematic of the electric setup. An image of an operating actuator is shown in Fig. 4. The visible purple strips next to electrodes are the plasma discharges. If this setup was operating in the wind tunnel, the flow would be from right to left.

B. Instrumentation

The flat plate had 45 static pressure taps, and a pitot tube was used to obtain the exit velocity. A Scanivalve Corporation 48-port J-type multiplexer was used with selective connections to two Druck (LPM 9381) differential pressure transducers of ± 0.1 kPa and ± 1 kPa ranges, respectively. The constant temperature anemometry (CTA) system used was A. A. Lab Systems AN-1003 with a 5 μm-diameter platinum wire. At each measurement location, 53 s-long time records were acquired, consisting of just over one million ($1{,}048{,}576 = 2^{20}$) data points collected at a 20 kHz sampling rate and using an antialiasing 8.3 kHz low-pass filter. An analog fiber-optic link (A. A. Lab Systems AFL-500) and an isolation transformer for the CTA system power supply were used for electric isolation.

C. Error Estimates

The uncertainty in mean and fluctuating velocities is 5%, which is primarily due to the bias error resulting from calibration uncertainty; see [6], which used a similar setup and system. Note that the velocity error is 0.5% for the Dantec jet calibrator used to calibrate the hotwire,

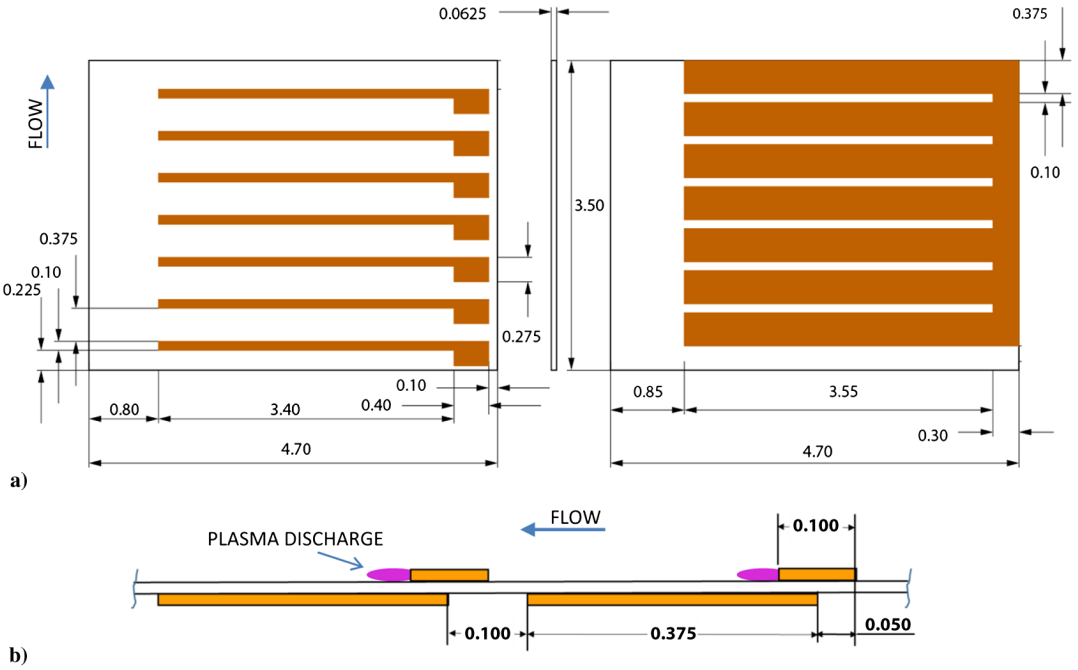

Fig. 2 Actuator design: a) top and bottom views; corners at figure center are the same flow direction from bottom to top, and b) detailed view of two electrode-pairs showing the offset. Dimensions are in inches.

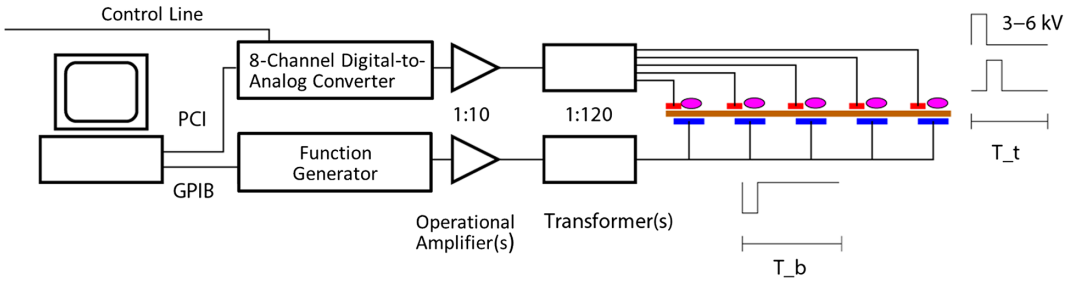

Fig. 3 Actuator and high-voltage driver system schematic (PCI, peripheral component interconnect; GPIB, general purpose interface bus).

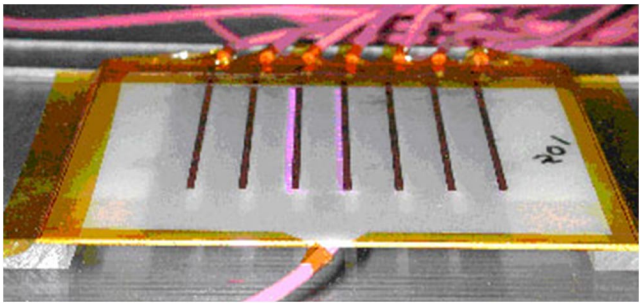

Fig. 4 Operating actuator: long exposure capturing two consecutive discharges.

the AN-1003 adds a voltage error of less than 0.1%, and 16-bit analog-to-digital conversion errors are made insignificant by signal pregain optimization. Essentially, the curve fit defining the calibration is the main source of the uncertainty. The Druck transducer's accuracy is a low 0.1% of full scale; hence, the uncertainty in the C_p values should not exceed 2% under the assumption that the transducers are not operated below one-tenth of its full-scale range (therefore, two transducers with different ranges were used).

III. Results and Interpretation

A. Pressure Measurements of the Base Flow (Plasma Off)

Streamwise pressure profiles for Reynolds numbers Re (based on L_s and the exit velocity) of 50,000, 100,000, 200,000, and 300,000 are shown in Fig. 5 along with the expected profile for the Pak-B airfoil. The pressure coefficients C_p, were computed from static pressure measurements using the exit velocity. The pressure profiles upstream of the throat were in good agreement with the Pak-B profile for all cases. Downstream, the agreement was good for the high-Reynolds-number Re, high-TI cases. At the lower Reynolds numbers, the C_p values indicated separation. At low TI and $Re = 50{,}000$, the boundary layer might not be fully reattached at $s/L_s = 1$, which is the end of the modeled airfoil.

B. Pressure Measurements with DBD Plasma Actuation Turned On

Figure 6 shows the impact on the C_p profile by operating the actuator with a typical $\Delta f = -49$ Hz for $Re = 50{,}000$ at low and high TIs. The horizontal line in Fig. 6a indicates the actuator location, and the dashes above this line show the location of the upper

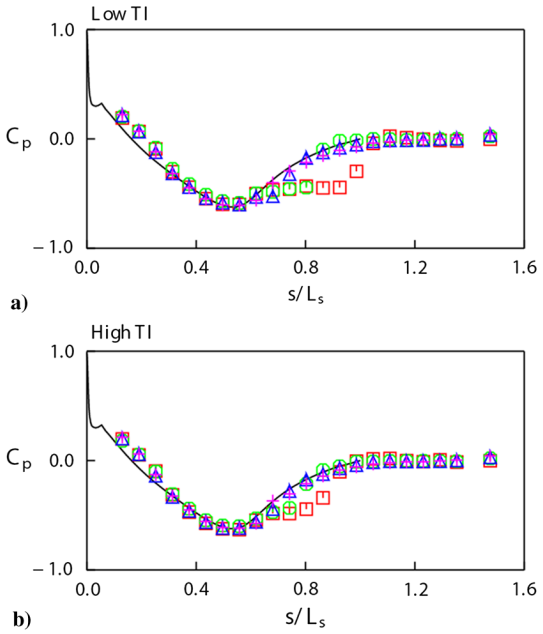

Fig. 5 C_p profiles: a) low TI and b) high TI; $Re = 50{,}0000$ (square), 100,000 (circle), 200,000 (triangle), and 300,000 (plus).

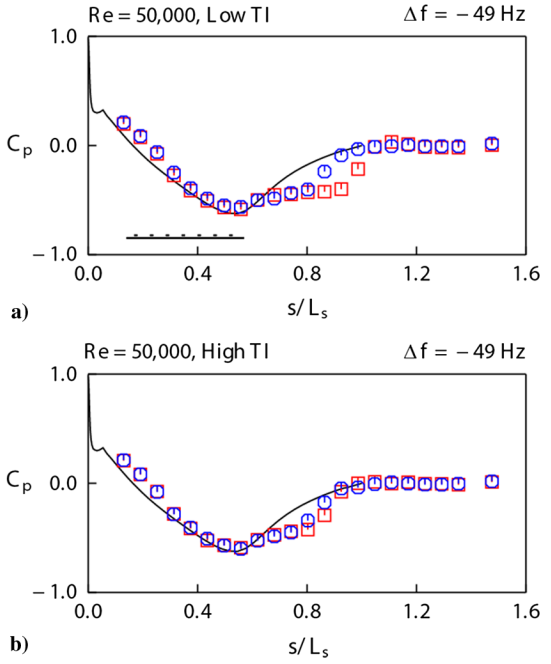

Fig. 6 C_p profiles: a) low TI, and b) high TI; actuator off (square) and on (circle).

electrodes. The plasma discharge forms at the downstream edge of these. As can be seen in the low-TI case (Fig. 6a), the separated region is reduced and the theoretical profile is recovered before the end of the modeled airfoil. In the high-TI case (Fig. 6b), the reduction of the separation is much less drastic; but, even here, an improvement can be seen.

The results were very similar for forcing frequencies $|\Delta f|$ between roughly 30 to 150 Hz. The corresponding frequency parameter F^+ ($|\Delta f|$ scaled with the suction surface distance between the pressure minimum and the trailing edge of the modeled airfoil and the nominal exit velocity) was about 0.6 to 3. The effectiveness was rather flat in this range and then gradually dropped off; it was still effective, but much less so, down to 10 Hz and up to 200 Hz. The sign of the delta frequency turned out not to change the effectiveness of the actuator.

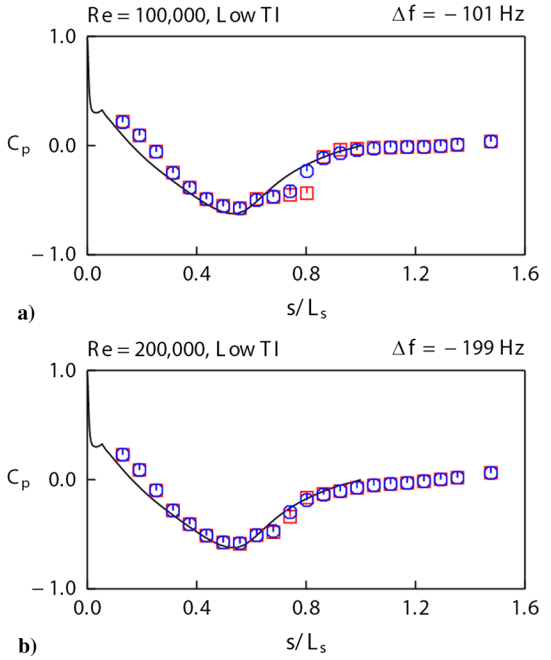

Fig. 7 C_p profiles with low TI: a) $\Delta f = -101$ Hz and $Re = 100{,}000$, and b) $\Delta f = -199$ Hz and $Re = 200{,}000$; actuator off (square) and on (circle).

That is, plasma forming sequentially in the upstream direction worked as well as in the downstream direction. This led to the conclusions that the effect was due to the forcing frequency and the direction of the oscillatory momentum input was immaterial.

Figure 7 shows the effect of operating the actuator for low TI and $Re = 100{,}000$ and 200,000 at $\Delta f = -101.36$ Hz and -199.16 Hz, respectively (resulting in F^+ close to the cases in Fig. 6). The effect of the actuator here is also to reduce the separated region. In the $Re = 200{,}000$ case, the unforced flow is nearly fully attached and the effect of the actuator is minimal.

The results indicate that the actuator works by promoting transition in the shear layer of the separation bubble, which then leads to earlier reattachment. This conclusion is further supported by the hot-wire measurements described next.

C. Hot-Wire Measurements

The mean streamwise velocity and streamwise fluctuating profiles are shown in Fig. 8 for stations 9–13 (coordinates listed in Table 1) for the low-TI $Re = 50{,}000$ case. Near-wall corrections of the hot-wire measurements were not made because the focus was on studying the effectiveness of the approach.

In the case of the actuator turned off, Fig. 8a (squares) shows that the boundary layer is clearly separated at stations 9 and 10 and that the separation bubble is growing. At stations 11 and 12, the low but nonzero velocities near the wall indicate that the boundary layer is beginning to reattach, although it may be intermittent. At station 13, representing the end of the simulated airfoil, the boundary layer is reattached. The corresponding fluctuating velocity profiles (squares) in Fig. 8b show very low turbulence at stations 9 and 10, with a slight increase in U_{RMS} just above the separation bubble. The U_{RMS} fluctuations continue to grow in the shear layer over the separation bubble at stations 9 through 12. The U_{RMS} level is still very low inside the bubble at stations 9 and 10, indicating that the flow is largely stagnant in this region. At station 11, significant U_{RMS} fluctuations also begin to appear near the wall. This indicates that the boundary layer is starting to reattach. The fluctuations are also extending farther from the wall toward the freestream. By the last station, the U_{RMS} profile shows significant fluctuations starting near the wall and well out into the freestream, indicating that transition in the shear layer over the separation bubble has reattached the flow.

When the actuator is turned on, Fig. 8 (circles) shows that reattachment starts already at station 9 and is completed by station 11. The separation bubble is thus much shorter and thinner. Consistent with this picture, significant unsteady fluctuations now also occur near the wall and well out into the freestream already at station 11. The broadening of the peak in the U_{RMS} distribution toward the wall from stations 11 through 13 indicates that an attached turbulent or transitional boundary layer is developing.

Table 1 Station locations

Station no.	s/L_s
1	0.28
2	0.33
3	0.39
4	0.45
5	0.51
6	0.57
7	0.63
8	0.69
9	0.75
10	0.81
11	0.88
12	0.94
13	1.00
14	1.06

The velocity profiles for the high-TI $Re = 50{,}000$ case are shown in Fig. 9. With the actuator off (squares), the boundary layer is separated at stations 9 and 10 but the thickness of the separation bubble is only about half that of the corresponding low-TI case at station 9. At station 11, the boundary layer has just reattached, and the profile shape recovers to that of an attached turbulent boundary layer through stations 12 and 13. In the corresponding low-TI case, reattachment does not occur until station 13. At station 9, the U_{RMS} profile shows a pronounced peak at the location of the maximum shear of the mean profile, i.e., in the shear layer over the separation bubble. This peak spreads toward the wall as the flow reattaches.

With the actuator turned on (circles), Fig. 9 shows that the reattachment process is moderately accelerated as compared to when it is off. However, the profiles at the last station are quite similar. This suggests that the actuator is most effective in modifying the flow in the shear layer above the separation bubble and that it has limited (if any) further effect once the flow has reattached.

Figures 10 and 11 show the evolution of the U' power spectral densities at the locations of maximum U_{RMS}. Figure 10a is for $Re = 50{,}000$, low TI, and the actuator turned off. The front curve (station 9) shows that the fluctuations mainly occur at very low

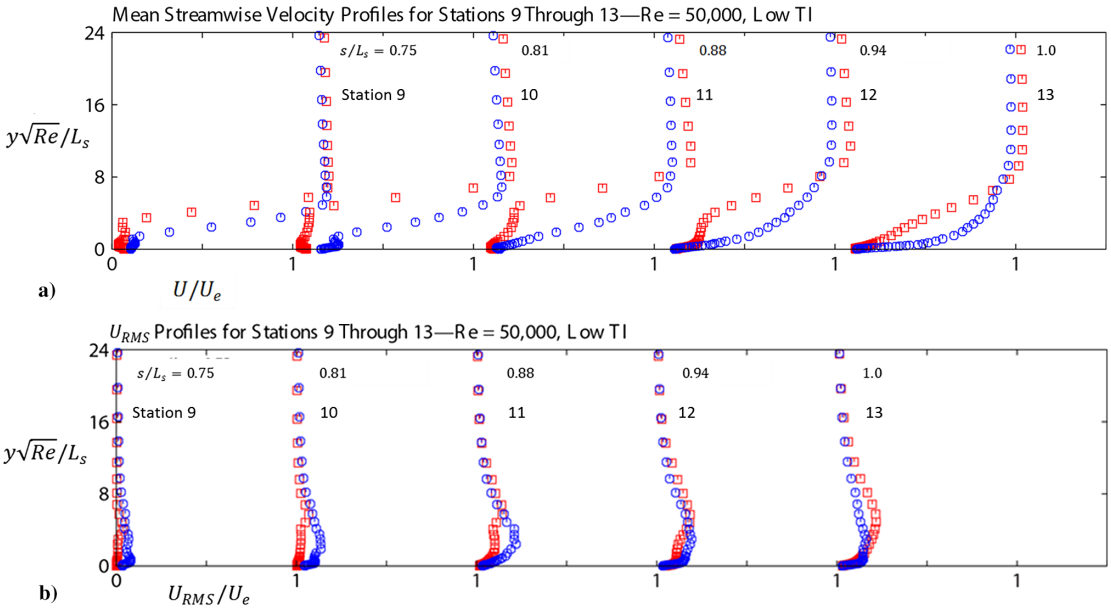

Fig. 8 Profiles for low-TI $Re = 50{,}000$ case: a) mean velocity and b) U_{RMS}; actuator off (square) and on (circle).

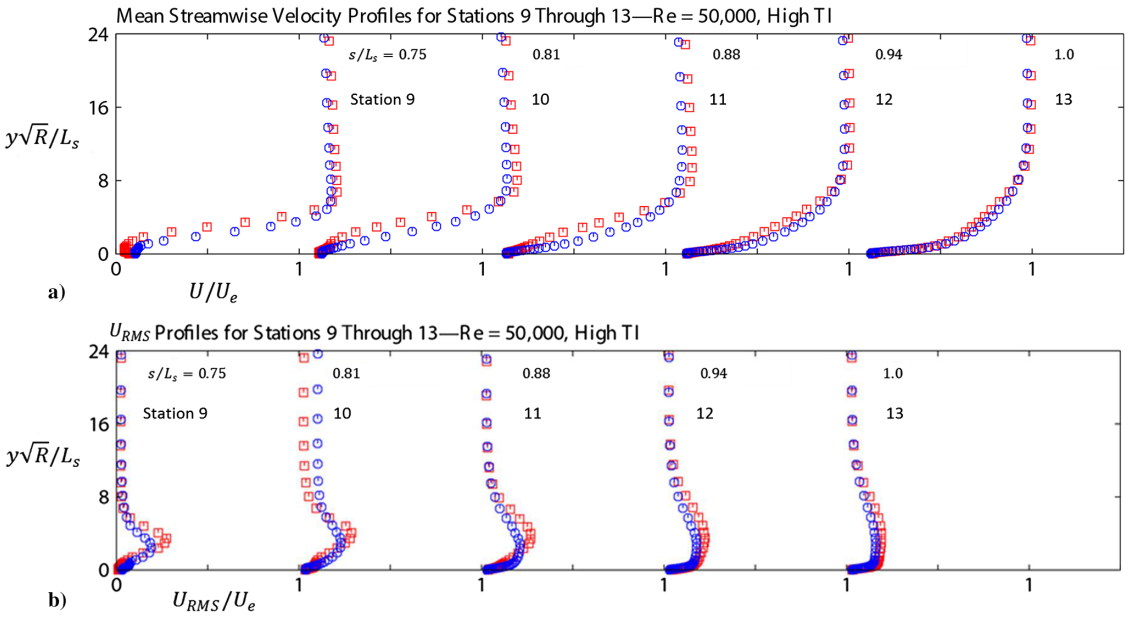

Fig. 9 Profiles for high-TI $Re = 50{,}000$ case: a) mean velocity, and b) U_{RMS}; actuator off (square) and on (circle).

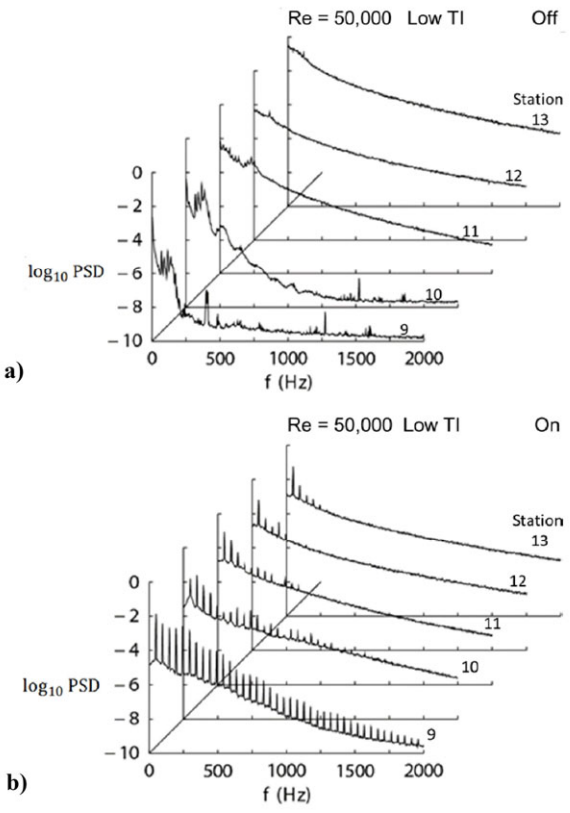

Fig. 10 U' power spectrum densities (PSDs) at locations of maximum U_{RMS} at stations 9–13 for low-TI $Re = 50{,}000$ case: a) actuator off, and b) actuator on.

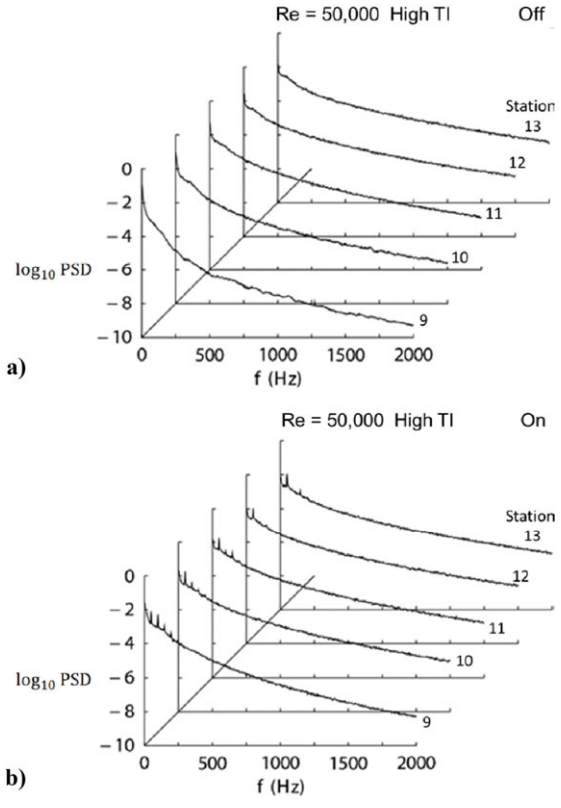

Fig. 11 U' power spectrum densities at locations of maximum U_{RMS} at stations 9–13 for high-TI $Re = 50{,}000$ case: a) actuator off, and b) actuator on.

frequencies and in a band centered about 125 Hz, with the latter due to shear layer instability. At higher frequencies, the magnitude is still low, indicating that the flow is not yet turbulent. At station 10, the shear layer instability increases in magnitude, significant higher harmonics are generated, and the shear layer is in late stages of transition. Between stations 10 and 11, there is a sudden jump to higher levels at higher frequencies, indicating a transition to turbulence. Thus, the shear layer is turbulent at stations 11 and 12. The curve for the last station 13, in combination with the corresponding results in Fig. 8, indicates reattached turbulent flow.

Figure 10b is with the actuator turned on. Distinct peaks at the unsteady forcing frequency and its harmonics can be seen in the curve for station 9. The overall shape of the curve is also of a turbulent nature. This suggests that the effect of the actuator is to have nearly,

if not already, transitioned the shear layer flow to turbulence at this station. At station 10, the increased level at the higher frequencies clearly indicates that the shear layer now is turbulent. The effective range of forcing frequencies noted in the previous subsection can now be understood in terms of the frequency band for instability waves in the separated shear layer. The later curves, in combination with the corresponding results in Fig. 9, indicate reattached turbulent flow at stations 11–13.

Figure 11a is for $Re = 50{,}000$, high TI, and the actuator turned off. Comparing to Fig. 10, there is considerably more fluctuation energy in the high-TI case at the first station than in the low-TI case. This energy is induced by the freestream over all frequencies, with no frequency spikes, but with lower frequencies more successful in penetrating the upstream boundary layer. This penetration, known to be induced by the freestream fluctuations [52–54] and detectable by a near-wall peak in the U_{RMS} distribution, occurs already at the stations upstream of the ones presented here. Volino and Hultgren [6] documented the slow but steady growth of these low-frequency disturbances through the favorable pressure gradient region upstream of the boundary-layer separation location, as well as their movement away from the wall and into the still laminar shear layer over the separation bubble. The later curves in Fig. 11a show no amplification of select instabilities as in Fig. 10a, but rather a rising energy level across the entire spectrum as transition proceeds. This indicates that transition occurs through a bypass mode rather than the breakdown of the instability waves seen in the low-TI case [6,53]. Downstream of transition, the spectra for the low- and high-TI cases are essentially the same.

Figure 11b is with the actuator on. The level at higher frequencies is increased at station 9 as compared to the unforced case in Fig. 11a, indicating that using the actuator accelerates the transition process. The curves at the last three stations are very similar for both cases in this figure, indicating the limited further effect of the forcing once transition to turbulence occurs.

IV. Conclusions

The effectiveness of active flow control of boundary-layer separation using a phased-array dielectric barrier discharge (DBD) plasma actuator has been documented under Reynolds number and pressure gradient conditions typical of low-pressure turbine airfoils. The results of pressure, velocity, fluctuation, and spectra measurements complemented each other, were mutually consistent, and enabled interpretation and identification of the flow control mechanisms, suggesting that the actuator worked by promoting early transition in the shear layer above the separation bubble, thus leading to rapid reattachment. The actuator was effective in a frequency band corresponding to the range of instability waves in the separated shear layer. It was particularly effective under low freestream turbulence conditions in which the boundary layer was laminar at separation. It also accelerated transition and subsequent reattachment under high freestream turbulence conditions in which the pretransitional boundary layer separated at about the same location as in the low freestream turbulence case and the shear layer transition occurred through a bypass mode. Comparisons to the cited experiments performed with standard AC-DBD actuators or to other active methods would have been desirable, but were not possible, because those tests were made at different Reynolds numbers Re, TIs, or geometries. In addition, meaningful actuator effectiveness comparisons should be made at the same power consumption, but this information had not been reported. The phased array used here was expected to use less power for the same effectiveness and to be particularly useful when the separation point varied with changes in the flow conditions.

Acknowledgments

The work was supported by the John H. Glenn Research Center's Director's Discretionary Fund and the NASA Transformative Aeronautics Concepts Program, Transformational Tools and Technologies Project. The authors wish to thank T. C. Corke and A. Aharoni for helpful advice and discussions.

References

[1] Suzen, Y. B., Huang, P. G., Ashpis, D. E., Volino, R. J., Corke, T. C., Thomas, F. O., Huang, J., Lake, J. P., and King, P. I., "A Computational Fluid Dynamics Study of Transitional Flows in Low-Pressure Turbines Under a Wide Range of Operating Conditions," *Journal of Turbomachinery*, Vol. 129, No. 3, 2007, pp. 527–541. doi:10.1115/1.2218888

[2] Mayle, R. E., "The Role of Laminar-Turbulent Transition in Gas Turbine Engines," *Journal of Turbomachinery*, Vol. 113, No. 4, 1991, pp. 509–537. doi:10.1115/1.2929110

[3] Hourmouziadis, J., "Aerodynamic Design of Low Pressure Turbines," AGARD Lecture Series 167, Neuilly-Sur-Seine, France, 1989.

[4] Sharma, O. P., Ni, R. H., and Tanrikut, S., "Unsteady Flow in Turbines," AGARD Lecture Series LS-195, Neuilly-Sur-Seine, France, 1994, Paper 5.

[5] Volino, R. J., "Separated Flow Transition Under Simulated Low-Pressure Turbine Airfoil Conditions: Part 1—Mean Flow and Turbulence Statistics," *Journal of Turbomachinery*, Vol. 124, No. 4, 2002, pp. 645–655. doi:10.1115/1.1506938

[6] Volino, R. J., and Hultgren, L. S., "Measurements in Separated and Transitional Boundary Layers Under Low-Pressure Turbine Airfoil Conditions," *Journal of Turbomachinery*, Vol. 123, No. 2, 2001, pp. 189–197. doi:10.1115/1.1350408

[7] Suzen, Y. B., Huang, P. G., Hultgren, L. S., and Ashpis, D. E., "Predictions of Separated and Transitional Boundary Layers Under Low-Pressure Turbine Airfoil Conditions Using an Intermittency Transport Equation," *Journal of Turbomachinery*, Vol. 125, No. 3, 2003, pp. 455–464. doi:10.1115/1.1580159

[8] Gad-el-Hak, M., *Flow Control, Passive, Active, and Reactive Flow Management*, Cambridge Univ. Press, Cambridge, England, U.K., 2000. doi:10.1017/cbo9780511529535

[9] Tiainen, J., Aki Grönma, A., Jaatinen-Värri, A., and Backman, J., "Flow Control Methods and Their Applicability in Low-Reynolds-Number Centrifugal Compressors—A Review," *International Journal of Turbomachinery, Propulsion and Power*, Vol. 3, No. 1, Dec. 2018, Paper 2. doi:10.3390/ijtpp3010002

[10] Volino, R. J., "Separation Control on Low-Pressure Turbine Airfoils Using Synthetic Vortex Generator Jets," *Journal of Turbomachinery*, Vol. 125, No. 4, 2003, pp. 765–777. doi:10.1115/1.1626686

[11] Sondergaard, R., "LPT Flow Control at AFRL," AIAA Paper 2008-4156, June 2008. doi:10.2514/6.2008-4156

[12] Lake, J. P., King, P. I., and Rivir, R. B., "Low Reynolds Number Loss Reduction on Turbine Blades with Dimples and V-Grooves," AIAA Paper 2000-0738, Jan. 2000. doi:10.2514/6.2000-738

[13] Volino, R. J., "Passive Flow Control on Low-Pressure Turbine Airfoils," *Journal of Turbomachinery*, Vol. 125, No. 4, 2003, pp. 754–764. doi:10.1115/1.1626685

[14] Bons, J., Sondergaard, R., and Rivir, R., "Control of Low-Pressure Turbine Separation Using Vortex Generator Jets," AIAA Paper 1999-0367, Jan. 1999. doi:10.2514/6.1999-367

[15] Bons, J. P., Sondergard, R., and Rivir, R. B., "Turbine Separation Control Using Pulsed Vortex Generator Jets," *Journal of Turbomachinery*, Vol. 123, No. 2, 2001, pp. 198–206. doi:10.1115/1.1350410

[16] Bons, J. P., Sondergaard, R., and Rivir, R. B., "The Fluid Dynamics of LPT Blade Separation Control Using Pulsed Jets," *Journal of Turbomachinery*, Vol. 124, No. 1, 2002, pp. 77–85. doi:10.1115/1.1425392

[17] Van Treuren, K. W., Simon, T., von Koller, M., Byerley, A. R., Baughn, J. W., and Rivir, R. B., "Measurements in a Turbine Cascade Flow Under Ultra Low Reynolds Number Conditions," *Journal of Turbomachinery*, Vol. 124, No. 1, 2002, pp. 100–106. doi:10.1115/1.1415736

[18] Bons, J. P., Reimann, D., and Bloxham, M., "Separated Flow Transition on an LP Turbine Blade with Pulsed Flow Control," *Journal of Turbomachinery*, Vol. 130, No. 2, 2008, Paper 021014. doi:10.1115/1.2751149

[19] Volino, R. J., Kartuzova, O., and Ibrahim, M. B., "Separation Control on a Very High Lift Low Pressure Turbine Airfoil Using Pulsed Vortex

Generator Jets," *Journal of Turbomachinery*, Vol. 133, No. 4, 2011, Paper 041021.
doi:10.1115/1.4003024

[20] Bons, J. P., Pluim, J., Gompertz, K., Bloxham, M., and Clark, J. P., "The Application of Flow Control to an Aft-Loaded Low Pressure Turbine Cascade with Unsteady Wakes," *Journal of Turbomachinery*, Vol. 134, No. 3, 2012, Paper 031009.
doi:10.1115/1.4000488

[21] Moreau, E., "Airflow Control by Non-Thermal Plasma Actuators," *Journal of Physics D: Applied Physics*, Vol. 40, No. 3, 2007, pp. 605–636.
doi:10.1088/0022-3727/40/3/S01

[22] Corke, T. C., Post, M. L., and Orlov, D. M., "SDBD Plasma Enhanced Aerodynamics: Concepts, Optimization and Applications," *Progress in Aerospace Sciences*, Vol. 43, Nos. 7–8, 2007, pp. 193–217.
doi:10.1016/j.paerosci.2007.06.001

[23] Corke, T. C., Post, M. L., and Orlov, D. M., "Single Dielectric Barrier Discharge Plasma Enhanced Aerodynamics: Physics, Modeling and Applications," *Experiments in Fluids*, Vol. 46, No. 1, 2009, pp. 1–26.
doi:10.1007/s00348-008-0582-5

[24] Corke, T. C., Enloe, C. L., and Wilkinson, S. P., "Dielectric Barrier Discharge Plasma Actuators for Flow Control," *Annual Reviews of Fluid Mechanics*, Vol. 42, No. 1, 2010, pp. 505–529.
doi:10.1146/annurev-fluid-121108-145550

[25] Benard, N., and Moreau, E., "Electrical and Mechanical Characteristics of Surface AC Dielectric Barrier Discharge Plasma Actuators Applied to Airflow Control," *Experiments in Fluids*, Vol. 55, No. 11, 2014, Paper 20141846.
doi:10.1007/s00348-014-1846-x

[26] Choi, K.-S., Jukes, T. N., Whalley, R. D., Feng, L., Wang, J., Matsunuma, T., and Segawa, T., "Plasma Virtual Actuators for Flow Control," *Journal of Flow Control, Measurement and Visualization*, Vol. 3, No. 1, 2015, pp. 22–34.
doi:10.4236/jfcmv.2015.31003

[27] Kotsonis, M., "Diagnostics for Characterisation of Plasma Actuators," *Measurement Science and Technology*, Vol. 26, No. 9, 2015, Paper 092001.
doi:10.1088/0957-0233/26/9/092001

[28] Kriegseis, J., Simon, B., and Grundmann, S., "Towards In-Flight Applications? A Review on Dielectric Barrier Discharge-Based Boundary-Layer Control," *Applied Mechanics Reviews*, Vol. 68, No. 2, 2016, Paper 020802.
doi:10.1115/1.4033570

[29] Roth, J. R., Sherman, D. M., and Wilkinson, S. P., "Electrohydrodynamic Flow Control with a Glow-Discharge Surface Plasma," *AIAA Journal*, Vol. 38, No. 7, 2000, pp. 1166–1172.
doi:10.2514/2.1110

[30] Enloe, C. L., McLaughlin, T. E., Van Dyken, R. D., Kachner, K. D., Jumper, E. J., and Corke, T. C., "Mechanisms and Responses of a Single Dielectric Barrier Plasma Actuator: Plasma Morphology," *AIAA Journal*, Vol. 42, No. 3, 2004, pp. 589–594.
doi:10.2514/1.2305

[31] Roupassov, D. V., Nikipelov, A. A., Nudnova, M. M., and Starikovskii, A. Y., "Flow Separation Control by Plasma Actuator with Nanosecond Pulsed-Periodic Discharge," *AIAA Journal*, Vol. 47, No. 1, 2009, pp. 168–185.
doi:10.2514/1.38113

[32] Opaits, D. F., Likhanskii, A. V., Neretti, G., Zaidi, S., Shneider, M. N., Miles, R. B., and Macheret, S. O., "Experimental Investigation of Dielectric Barrier Discharge Plasma Actuators Driven by Repetitive High-Voltage Nanosecond Pulses with DC or Low Frequency Sinusoidal Bias," *Journal of Applied Physics*, Vol. 104, No. 4, 2008, Paper 043304.
doi:10.1063/1.2968251

[33] Starikovskiy, A., Gordon, S., Post, M., and Miles, R., "Barrier Discharge Development and Thrust Generation at Low and High Pressure Conditions," AIAA Paper 2014-0329, Jan. 2014.
doi:10.2514/6.2014-0329

[34] Boxx, I., Rivir, R., Newcamp, J., and Woods, N., "Reattachment of a Separated Boundary Layer on a Flat Plate in a Highly Adverse Pressure Gradient Using a Plasma Actuator," AIAA Paper 2006-3023, June 2006.
doi:10.2514/6.2006-3023

[35] Burman, D., Simon, T., Kortshagen, U., and Ernie, D., "Separation Control Using Plasma Actuators: 2-D and Edge Effects in Steady Flow in Low Pressure Turbines," AIAA Paper 2010-1220, Jan. 2010.
doi:10.2514/6.2010-1220

[36] Burman, D., Simon, T. W., Kortshagen, U., and Ernie, D., "Separation Control Using Plasma Actuators: Steady Flow in Low Pressure Turbines," ASME Paper GT2011-46807, New York, June 2011.
doi:10.1115/gt2011-46807

[37] Matsunuma, T., and Segawa, T., "Effects of Input Voltage on Flow Separation Control for Low-Pressure Turbine at Low Reynolds Number by Plasma Actuators," *International Journal of Rotating Machinery*, Vol. 2012, 2012, Paper 902548.
doi:10.1155/2012/902548

[38] Pescini, E., Marra, F., De Giorgi, M. G., Francioso, L., and Ficarella, A., "Investigations of the Actuation Effect of a Single DBD Plasma Actuator for Flow Separation Control Under Simulated Low-Pressure Turbine Blade Conditions," ASME Paper GT2016-57432, New York, June 2016.
doi:10.1115/gt2016-57432

[39] List, J., Byerley, A., McLaughlin, T., and Van Dyken, R., "Using Plasma Actuators Flaps to Control Laminar Separation on Turbine Blades in a Linear Cascade," AIAA Paper 2003-1026, Jan. 2003.
doi:10.2514/6.2003-1026

[40] Huang, J., Corke, T. C., and Thomas, F. O., "Plasma Actuators for Separation Control of Low-Pressure Turbine Blades," *AIAA Journal*, Vol. 44, No. 1, 2006, pp. 51–57.
doi:10.2514/1.2903

[41] Huang, J., Corke, T. C., and Thomas, F. O., "Unsteady Plasma Actuators for Separation Control of Low-Pressure Turbine Blades," *AIAA Journal*, Vol. 44, No. 7, 2006, pp. 1477–1487.
doi:10.2514/1.19243

[42] Marks, C. R., Sondergaard, R., Wolff, M., and Anthony, R., "Experimental Comparison of DBD Plasma Actuators for Low Reynolds Number Separation Control," *Journal of Turbomachinery*, Vol. 135, No. 1, 2012, Paper 011024.
doi:10.1115/1.4006517

[43] Corke, T. C., and Matlis, E., "Phased Plasma Arrays for Unsteady Flow Control," AIAA Paper 2000-2323, June 2000.
doi:10.2514/6.2000-2323

[44] Wilkinson, S., "Oscillating Plasma for Turbulent Boundary Layer Drag Reduction," AIAA Paper 2003-1023, Jan. 2003.
doi:10.2514/6.2003-1023

[45] Roth, J. R., Madhan, R. C. M., Yadav, M., Rahel, J., and Wilkinson, S., "Flow Field Measurements of Paraelectric, Peristaltic, and Combined Plasma Actuators Based on the One Atmosphere Uniform Glow Discharge Plasma (OAUGDP®)," AIAA Paper 2004-0845, Jan. 2004.
doi:10.2514/6.2004-845

[46] Whalley, R. D., and Choi, K.-S., "Turbulent Boundary-Layer Control with Plasma Spanwise Travelling Waves," *Experiments in Fluids*, Vol. 55, No. 8, 2014, Paper 1796.
doi:10.1007/s00348-014-1796-3

[47] Post, M. L., "Phased Plasma Actuators for Unsteady Flow Control," M.S. Thesis, Univ. of Notre Dame, Notre Dame, IN, 2001.

[48] Hultgren, L. S., and Ashpis, D. E., "Glow Discharge Plasma Active Control of Separation Control at Low Pressure Turbine Conditions," *Bulletin of the American Physical Society*, Vol. 47, No. 10, 2002, Paper 167.

[49] Sohn, K. H., DeWitt, K. J., and Shyne, R. J., "Experimental Investigation of Boundary Layer Behavior in a Simulated Low Pressure Turbine," ASME Paper 98-GT-034, New York, June 1998.
doi:10.1115/98-gt-034

[50] Halstead, D. E., Walker, G. J., Wisler, D. C., Hodson, H. P., Okiishi, T. H., and Shin, H.-W., "Boundary Layer Development in Axial Compressors and Turbines: Part 3 of 4—LP Turbines," *Journal of Turbomachinery*, Vol. 119, No. 2, 1997, pp. 225–246.
doi:10.1115/1.2841105

[51] Hultgren, L. S., and Ashpis, D. E., "Demonstration of Separation Delay with Glow-Discharge Plasma Actuators," AIAA Paper 2003-1025, Jan. 2003; also NASA TM-2003-212204/REV1, Dec. 2004.
doi:10.2514/6.2003-1025

[52] Dryden, H. L., "Air Flow in the Boundary Layer near a Plate," NACA Rept. 562, 1936.

[53] Blair, M. F., "Boundary-Layer Transition in Accelerating Flow with Intense Freestream Turbulence: Part 1—Disturbances Upstream of Transition Onset," *Journal of Fluids Engineering*, Vol. 114, No. 3, 1992, pp. 313–321.
doi:10.1115/1.2910032

[54] Volino, R. J., "A New Model for Free-Stream Turbulence Effects on Boundary Layers," *Journal of Turbomachinery*, Vol. 120, No. 3, 1998, pp. 613–620.
doi:10.1115/1.2841760